NASA TECHNICAL MEMORANDUM

NASA TM X-3015

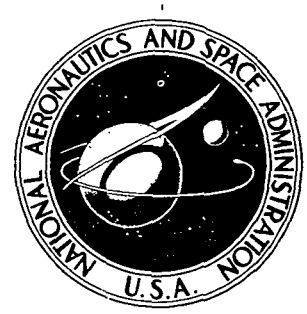

NASA TM X-3015

DRAG AND DISTRIBUTION MEASUREMENTS OF SINGLE-ELEMENT FUEL INJECTORS FOR SUPERSONIC COMBUSTORS

by Louis A. Povinelli

Lewis Research Center
Cleveland, Ohio 44135

NATIONAL AERONAUTICS AND SPACE ADMINISTRATION • WASHINGTON, D. C. • MARCH 1974

1. Report No.	2. Government Accession No.	3. Recipient's Catalog No.
NASA TM X-3015		

4. Title and Subtitle	5. Report Date
DRAG AND DISTRIBUTION MEASUREMENTS OF SINGLE-ELEMENT FUEL INJECTORS FOR SUPERSONIC COMBUSTORS	MARCH 1974
	6. Performing Organization Code

7. Author(s)	8. Performing Organization Report No.
Louis A. Povinelli	E-7662
	10. Work Unit No. 501-24

9. Performing Organization Name and Address	11. Contract or Grant No.
Lewis Research Center National Aeronautics and Space Administration Cleveland, Ohio 44135	

12. Sponsoring Agency Name and Address	13. Type of Report and Period Covered
National Aeronautics and Space Administration Washington, D.C. 20546	Technical Memorandum
	14. Sponsoring Agency Code

15. Supplementary Notes

16. Abstract

The drag caused by several vortex generating fuel injectors for scramjet combustors was measured in a Mach 2 to 3.5 airstream. Injector drag was found to be strongly dependent on injector thickness ratio. The distribution of helium injected into the stream was measured both in the near field and the far field of the injectors for a variety of pressure ratios. The far field results differed appreciably from measurements in the near field. Injection pressure ratio was found to profoundly influence the penetration. One of the aerowing configurations tested yielded low drag consistent with desirable penetration and spreading characteristics.

17. Key Words (Suggested by Author(s))	18. Distribution Statement
Scramjets; Hypersonic propulsion; Jet penetration; Aerodynamic drag; Scramjet fuel injectors	Unclassified - unlimited Cat. 12

19. Security Classif. (of this report)	20. Security Classif. (of this page)	21. No. of Pages	22. Price*
Unclassified	Unclassified	23	$2.75

* For sale by the National Technical Information Service, Springfield, Virginia 22151

DRAG AND DISTRIBUTION MEASUREMENTS OF SINGLE-ELEMENT FUEL INJECTORS FOR SUPERSONIC COMBUSTORS

by Louis A. Povinelli

Lewis Research Center

SUMMARY

Previous work has demonstrated that vortex motion in the leeward region of delta wing injectors can aid jet penetration and mixing in a supersonic stream. This report presents further results obtained with the same injector geometries. These injectors had sharp leading edges swept back at 58.5° and were mounted at 10° to 20° angles of attack to the flow. Helium was injected into or near the vortex region. The far field distribution of injectant was determined at Mach 2.5 for a variety of injectors. Injection- to free-stream-total-pressure ratios used were 6.2, 3.05, and 1.26. Both windward and leeward injection was investigated using a single hole, multiple holes, and a porous injection surface.

Drag measurements were made over a Mach number range from 2 to 3.5 with the injectors at 12° and 20° angles of attack. The experimental drag data at 12° and Mach 2 were compared with the results of linear theory. The delta wing injector with an inboard edge angle of about 6° was found to exhibit low drag and favorable penetration characteristics.

The tests were conducted at Mach 2.0, 2.5, 3.0, and 3.5 (nominal) in a 0.305- by 0.305-meter (1- by 1-ft) (cross section) wind tunnel. The total temperature of the air was 294 K (530° R), and the total pressure was varied from 100 to 134 kN/m^2 (14.5 to 19.5 psia). The dynamic pressure of the airstream was varied from 35.8 to 60.4 kN/m^2 (748 to 1262 psfa).

INTRODUCTION

This report is concerned with the measurement of drag and injectant distribution and spreading for scramjet fuel injectors. The future design of scramjet propulsion engines may include the use of hydrogen fuel injector struts, either protruding into or

spanning the combustor. These struts would be swept in the flow direction in order to reduce drag and heat transfer (ref. 1). The struts may also provide some internal compression and expansion surfaces in order to provide shock attenuation (ref. 2). It may also be possible to generate a vortex flow field (e.g., using swept edge at angle of attack) which could be utilized for enhancing jet penetration and mixing. Previous studies have demonstrated the feasibility of vortex enhancing jet penetration (refs. 3 to 5). Those studies (with the exception of ref. 3) were confined to determining the distribution of injectant in the near field region of a single-element injector. This limitation was required to avoid interference effects caused by the reflection of the model shock waves from the boundary layer on the tunnel side wall. This report presents spreading data for the far field which was obtained in a larger wind tunnel, free of interference effects. Drag of various injector shapes was also measured because of its importance in scramjet combustor design.

The tests were conducted at Mach 2.0, 2.5, 3.0, and 3.5 (nominal) in a 0.305- by 0.305-meter (1- by 1-ft) (cross section) wind tunnel. The total temperature of the air was 294 K (530° R) and the total pressure was varied from 100 to 134 kN/m^2 (14.5 to 19.5 psia).

APPARATUS AND PROCEDURE

Wind Tunnel and Fuel Injectors

The fuel injector models are shown in figure 1. (These same models were used in previous testing with a different support structure (refs. 5 and 6).) The models were identical except for a cutout section along the inboard edge. In addition to the configurations shown, model B was modified twice. A sintered porous injection strip was also used with model C, as shown in figure 2. The first modification to model B, shown in figure 3(a), was to drill five additional orifices (0.198 cm or 0.079 in. diam.) in the leeward surface along the centerline of the vortex region. In this case the injection velocity was subsonic. The second modification was to close the leeward orifices and drill three passages (0.152 cm or 0.060 in. diam.) beneath the swept edge (fig. 3(b)). The three orifices were drilled at an angle (56°) which corresponded to the angle of oil streak lines found on the windward surfaces. (With both of these modifications the combined orifice areas exceeded the plenum area. Hence the amount of injection through each orifice may vary. The resulting effect on fuel distribution was not ascertained.)

All the injectors had subsonic leading edges for the test conditions used. The component of a Mach 3 free stream normal to the 58.5° sweptback leading edge at a 12° angle of attack is 1.94. However, the sum of the wedge angle of the leading edge (24.8°) and the angle of incidence of the component normal to the leading edge (22°) is so large

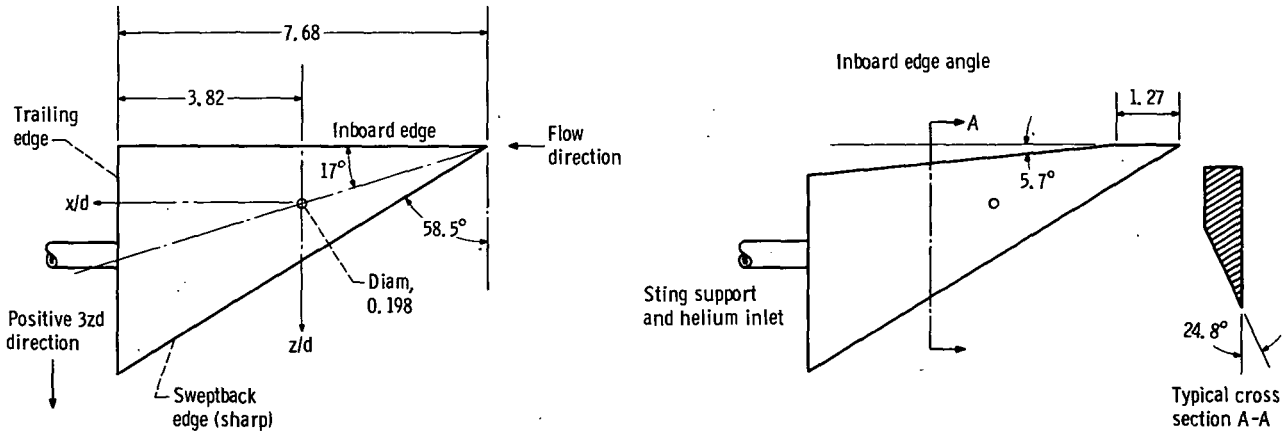

(a) Planform views (viewed normal to leeward surface).

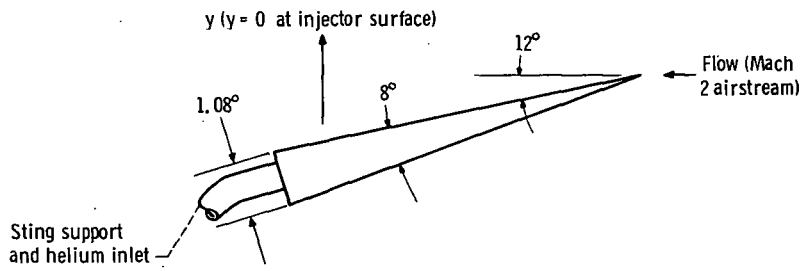

(b) Side view.

Figure 1. - Delta and arra wing injectors. (Dimensions in cm unless indicated otherwise.)

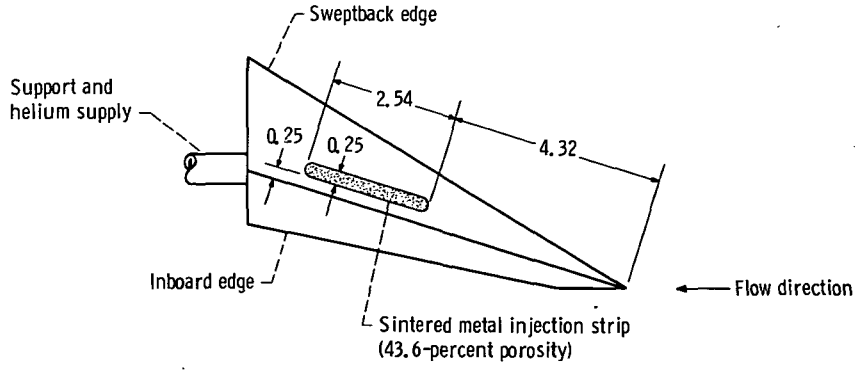

Figure 2. - Windward view of injector configuration C showing sintered injection strip. Angle of attack, 18°.

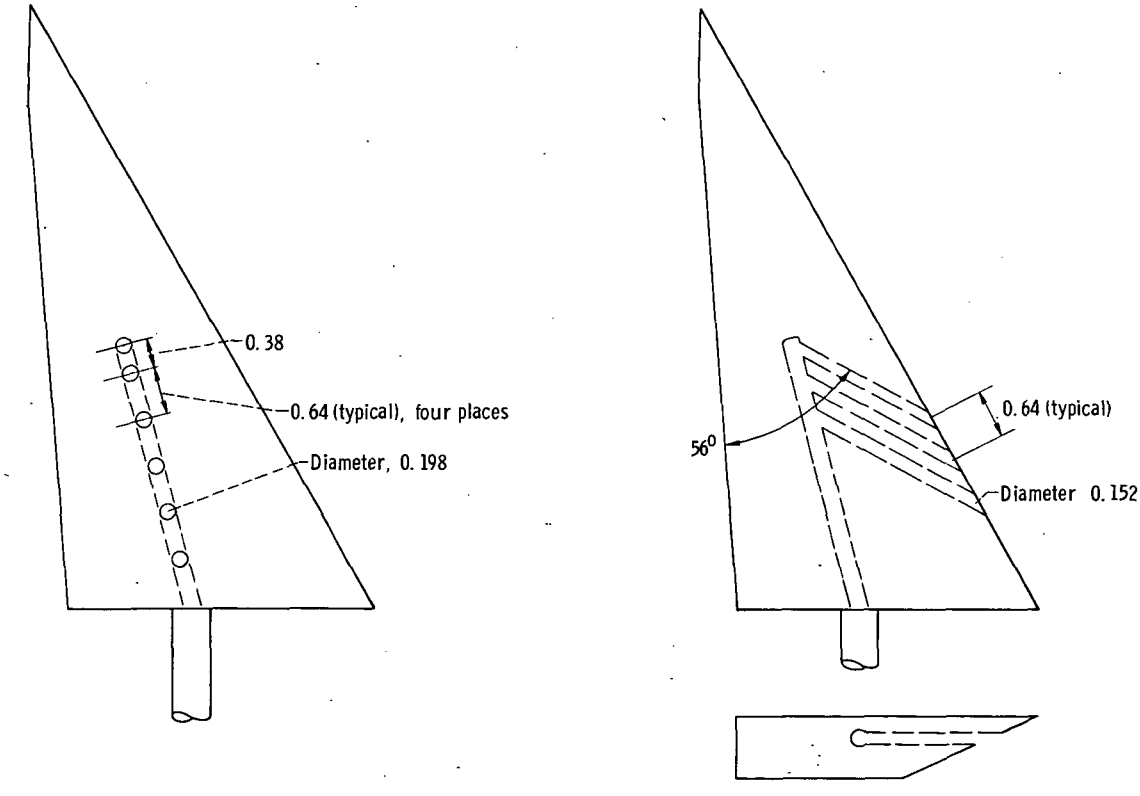

(a) Multiple leeward orifices.

(b) Drilled leading edge.

Figure 3. - Injector configuration B modified. (Dimensions in cm unless indicated otherwise.)

that the leading edge shock wave is detached. Hence, circulation occurs from the windward to the leeward side of the injectors and gives rise to vortex motion.

The injectors were mounted on a sting support mechanism capable of translation in three directions. Tests were conducted primarily at 14° and 18° angles of attack. The coordinate system used in this study was as follows. The downstream direction x was measured from the injection orifice parallel to the undisturbed free stream. (Symbols are defined in appendix A.) The lateral distance z was also measured from the orifice normal to the free stream with the positive direction towards the sweptback edge. Vertical distance y was measured from the injector surface in a direction perpendicular to the undisturbed stream. In the case of measurements downstream of the trailing edge, y was measured from the projection of the leeward trailing edge parallel to the free stream. All distances were nondimensionalized by the injection orifice diameter d (0.198 cm). For the porous strip injector, the origin of the coordinate system was assumed to be identical to that of injector A.

Helium was used to simulate hydrogen injection. Injection- to free-stream-total-pressure ratios were 6.2, 3.05, and 1.26.

Injectant Distribution Measurement

Samples were withdrawn from the flow stream using a wedge rake with 15 probe tips. Each tip was made of 0.076-centimeter- (0.030-in.-) outside diameter stainless tube with 0.0076-centimeter (0.003-in.) wall and protruded forward from the wedge a distance of 0.152 centimeter (0.06 in.). The center-to-center distance of the probe tips was 0.508 centimeter (0.2 in.). The probe tips were connected to a 12 position scanning valve (rendering three of the tips inoperative).

The sampling rake was moved in the vertical direction y using an actuator mechanism. Near field measurements were made at the trailing edge of the injectors (x/d = 19) and as far downstream as 123 diameters. The samples were continuously analyzed by a mass spectrometer for the amount of helium present in the sample. Sampling pressure was manually regulated to maintain a value of 20 torr (20 mm Hg abs). The sampling technique used has been described previously (ref. 4).

The position at which the helium concentration reached zero percent was recorded as the outer boundary of the jet plume. This boundary was taken as the location of maximum jet penetration. (Detailed concentration contours for the near field (x/d = 19) are presented in ref. 6 for the model shown in figs. 1 and 2.)

Drag Measurements

A photograph of the drag balance designed and constructed for this study is shown in figure 4. The injectors were mounted in the forward (moveable) portion of the balance. Linear bearings allow the undercarriage portion of the balance to move relative to the fixed (overcarriage) portion of the balance. A small load cell (222.4 N or 50 lbf) was mounted between the fixed and moveable parts of the balance. A split shroud was used

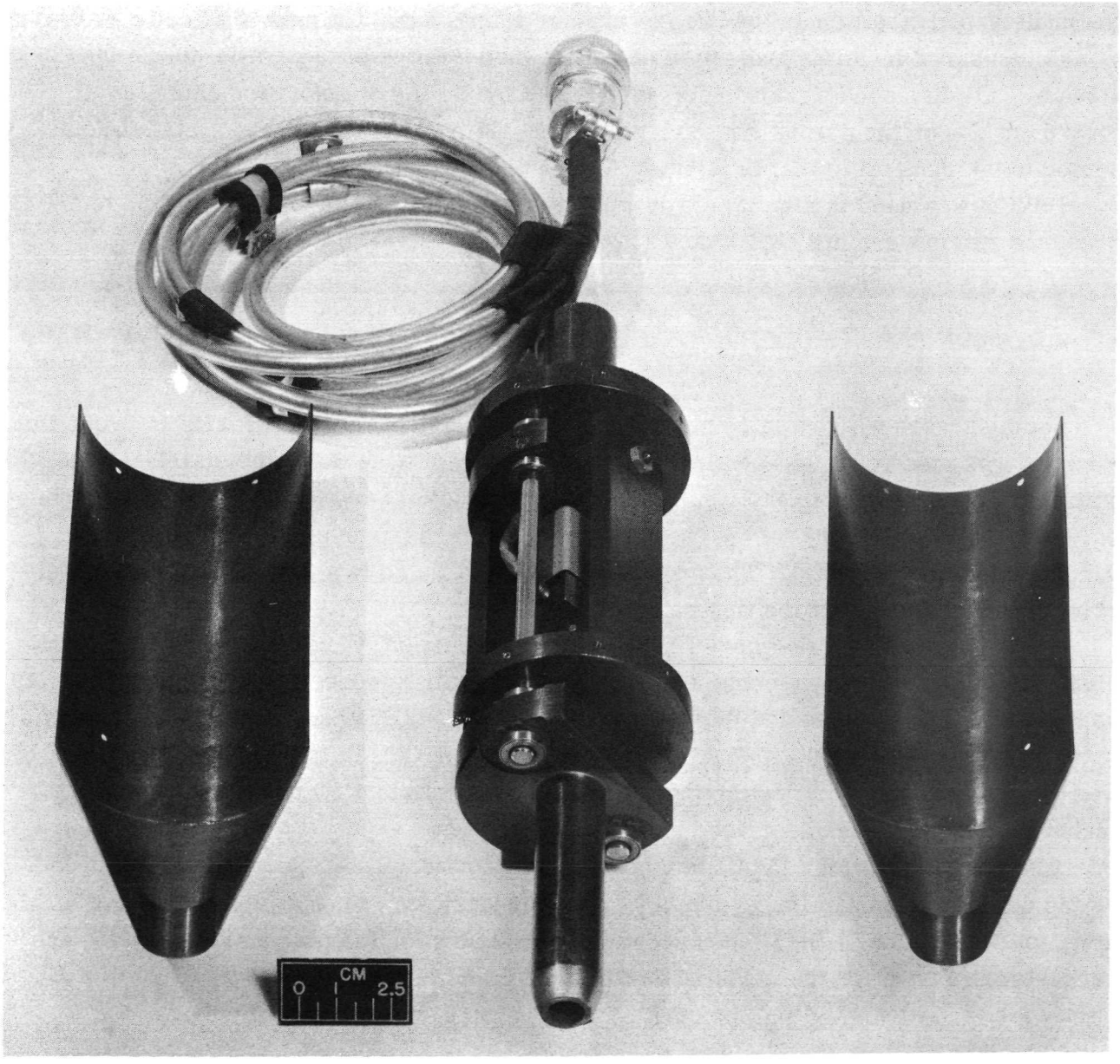

C-72-2468

Figure 4. - Drag balance split shroud removed.

to enclose the balance and was fastened to the fixed portion. The rear support rod then mounted into a sting support in the tunnel. Calibration of the drag balance was carried out using dead weights. Additional calibrations were made subsequent to tunnel operation to assess the effect of test section temperature on load cell reading. No significant variation of output was found over the period of time used in the tests.

RESULTS AND DISCUSSION

Flow Visualization

A schlieren photograph of the flow field around injector B is shown in figure 5. The edge view in figure 5(a) was made while helium was being injected (P_{oj} = 788 kN/m^2 or 114.5 psia). The main features in the edge view are the windward compression shock and the leeward injection shock upstream of the orifice. The expansion and recompression waves over the trailing edge of the injector are also evident. The remainder of the waves are caused by various portions of the model support sting and injection tubing.

The planar view is shown in figure 5(b). The strong windward compression wave is observed in the lower half of the photograph. The leeward shock upstream of the injec-

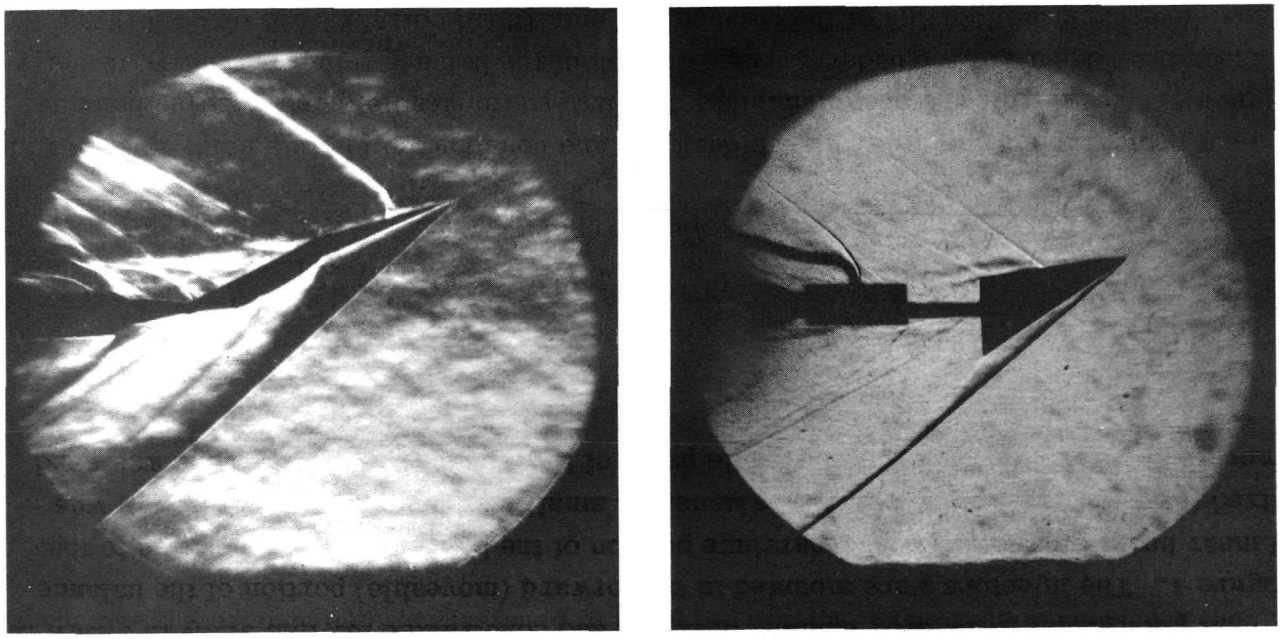

(a) Edge view.

(b) Planar view.

Figure 5. - Schlieren photograph of injector B; Mach 2 free stream. Helium injection at 788 kN/m^2 (114.5 psia); angle of attack, 12°; flow, right to left.

tion orifice is seen in the upper part of the photograph. Further downstream, the waves corresponding to the support sting are also visible.

Drag Measurements

The experimental results are shown in figure 6. Injector A (the half-delta configuration) yielded the largest drag. Reducing the surface area of the injector (A to B) caused a 37 percent decrease in the drag. However, a further reduction of the area (B to C to D) caused an increase in drag. The support drag was obtained by removing one of the plan forms from the sting and measuring the resulting drag. Comparison of the experimental data with calculated drag values (see appendix B) is given in figure 7. Quantitatively, the results with injectors A and D appear to correspond to the linear calculations whereas with injectors B and C, there is both qualitative and quantitative disagreement. The trend of the experimental results and the lack of agreement with calculations prompted further testing. Injector D was modified so that its thickness ratio (midpoint thickness/chord length) was equal to that of injector B. This change would be

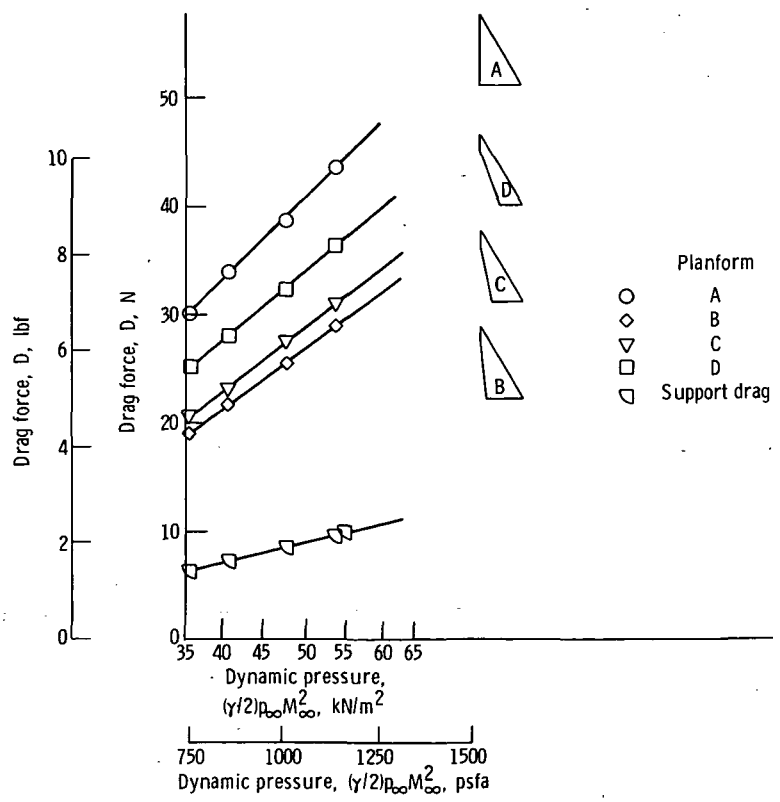

Figure 6. - Experimental drag measurements. Mach number, 2.0; angle of attack, 12°.

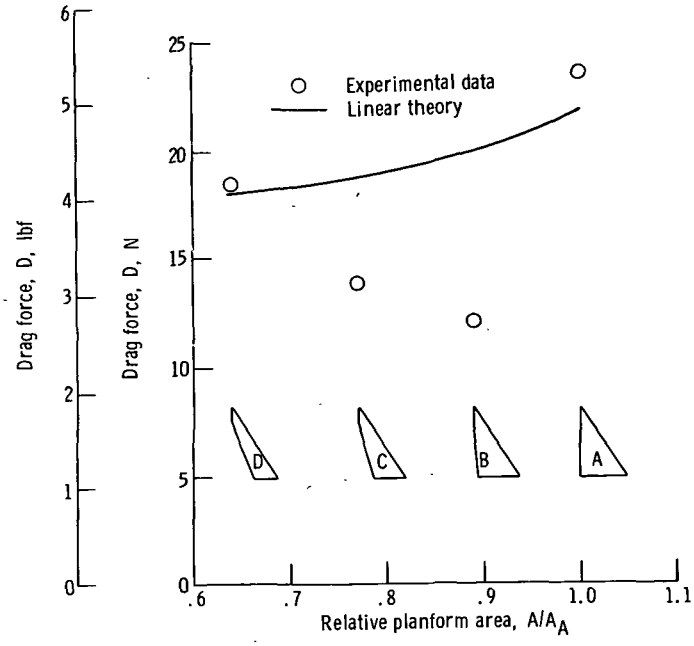

Figure 7. - Comparison of calculated and measured drag. Mach number, 2.0; angle of attack, 12°.

expected to reduce the thickness drag as well as the base drag. The experimental result is shown in figure 8. The measured drag for injector D approximates that of injector B. Since the thickness drag of the modified injector D is equal to that of B and the base drag of D is less than that of B, the presence of a vortex flow field must be influencing the drag forces. It is known that the existence of vortex flow can lead to regions of low pressure in the flow field. This nonuniformity of the flow may be responsible for the difference between the experimental data and the linear drag calculations.

Drag measurements were made while helium was being injected (injection total pressure ≤ 1070 kN/m^2 or 155 psia) into the flow stream. The effect of gas injection on the measured drag was found to be negligible. The calculated change in drag due to the momentum of the injected helium was only 2 percent.

The drag of injector B was also measured over the range of Mach numbers from 2.0 to 3.5. The free-stream dynamic pressure was varied from 37.9 to 48.3 kN/m^2 (792 to 1008 psia) as shown in figure 9. Over the Mach number range studied the drag does not vary a great deal. The data at 12° angle of attack shows a slightly greater dependence on Mach number than that at 20°.

The results obtained indicate that injector D creates as much drag as injector B and does not, therefore, present any apparent advantage over injector B. The penetration and spreading characteristics must now be considered in comparing these injectors.

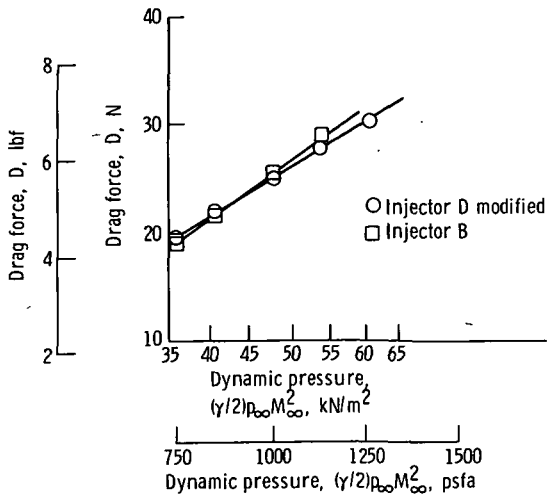

Figure 8. - Experimental drag measurements. Mach number, 2.0; angle of attack, 12°; equal thickness ratios.

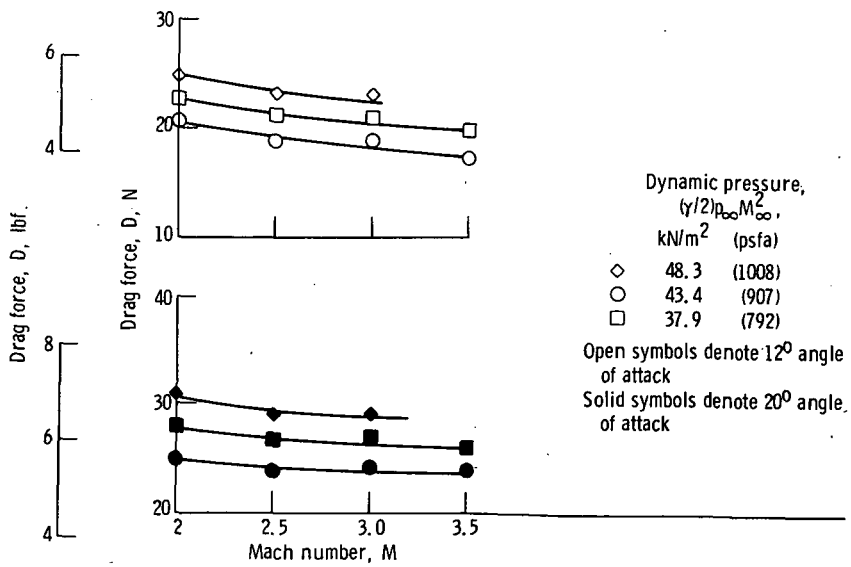

Figure 9. - Drag measurements at various Mach numbers and dynamic pressures. Injector B.

Jet Penetration

Injector B

The effect of injection- to free-stream-total-pressure ratio on jet penetration is shown in figure 10(a), (b), and (c), for various downstream positions. These tests were performed with injector B oriented at 14^{o} angle of attack in a Mach 2.5 airstream. Figure 10(a) shows that the maximum near field penetration (i.e., zero percent helium boundary) occurs at a z/d position of approximately zero. Further downstream the distribution flattens and the central portion of the curve shifts toward the vortex position, occurring at a z/d of 2. More significantly, the penetration in the vortex region (z/d $\approx$ 11) increases as one moves further downstream. This far field distribution is markedly different than that of the near field. Decreasing the total pressure ratio from 6.2 to 3.05 yields the change shown in figure 10(b). The far field now differs considerably from the near field distribution but, additionally, it bears little resemblance to the higher pressure ratio data of figure 10(a). The same remark applies to the data in figure 10(c) for a pressure ratio of 1.26. In this case, a stretching and breaking of the downstream plume can be seen, one portion corresponding to the main jet position, the other corresponding to the vortex position.

The foregoing results for three downstream stations are replotted in figure 11 with pressure ratio as the variable parameter. Figure 11(a) shows that jet penetration at a fixed downstream position (x/d = 19) increases with pressure ratio in the region directly downstream of the injection orifice, z/d = 0 (central jet region), whereas the penetration at the vortex position, z/d = 11 (vortex region), is hardly affected by the pressure ratio. This behavior is more clearly described by the near field plot in figure 12. Jet penetration is plotted as a function of pressure ratio for various cross stream positions. The strong dependence of penetration on pressure ratio is seen in the central jet region (z/d from 0 to 5) whereas the penetration in the vortex region (z/d of 8 to 12) is virtually independent of the pressure ratio. At the downstream positions (x/d = 75 and 100 in figure 11(b) and (c), there is some dependency of vortex penetration on pressure ratio. This dependency, however, is far less than that of the central jet region.

The results indicate that the distribution of helium may vary over a wide range depending on pressure ratio. In addition, the downfield distribution appears to bear little resemblance to the near field results, particularly at the lower pressure ratios. Accordingly, subsequent tests in this study were made with a pressure ratio of 1.26 (a realistic value for scramjet combustors). In addition, no reliance was placed on the near field results for the prediction of the far field behavior.

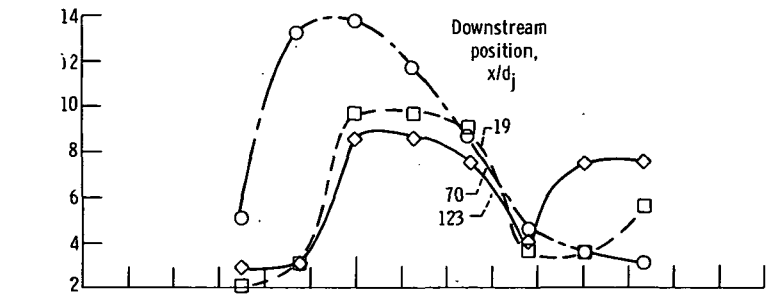

(a) Injectant- to free-stream-pressure ratio, 6.2.

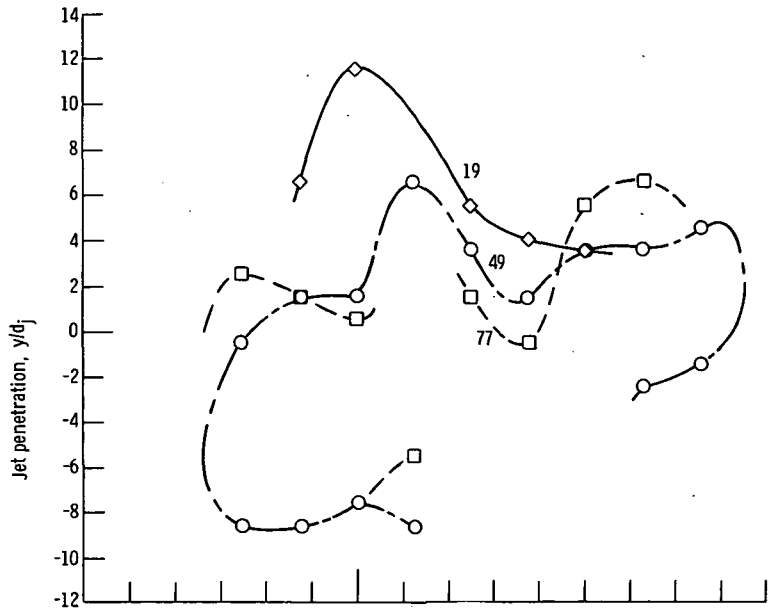

(b) Injectant- to free-stream-pressure ratio, 3.05.

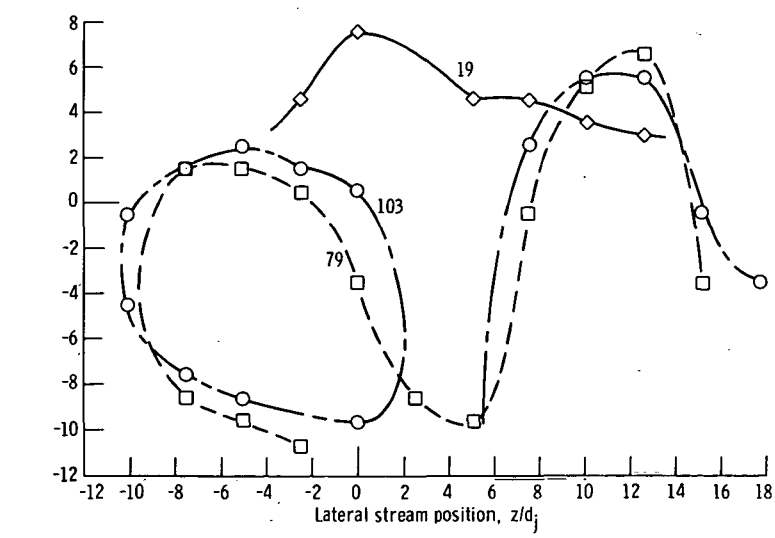

(c) Injectant- to free-stream-pressure ratio, 1.26.

Figure 10. - Jet penetration at various downstream positions. Mach number, 2.5; angle of attack, 14^0; model B.

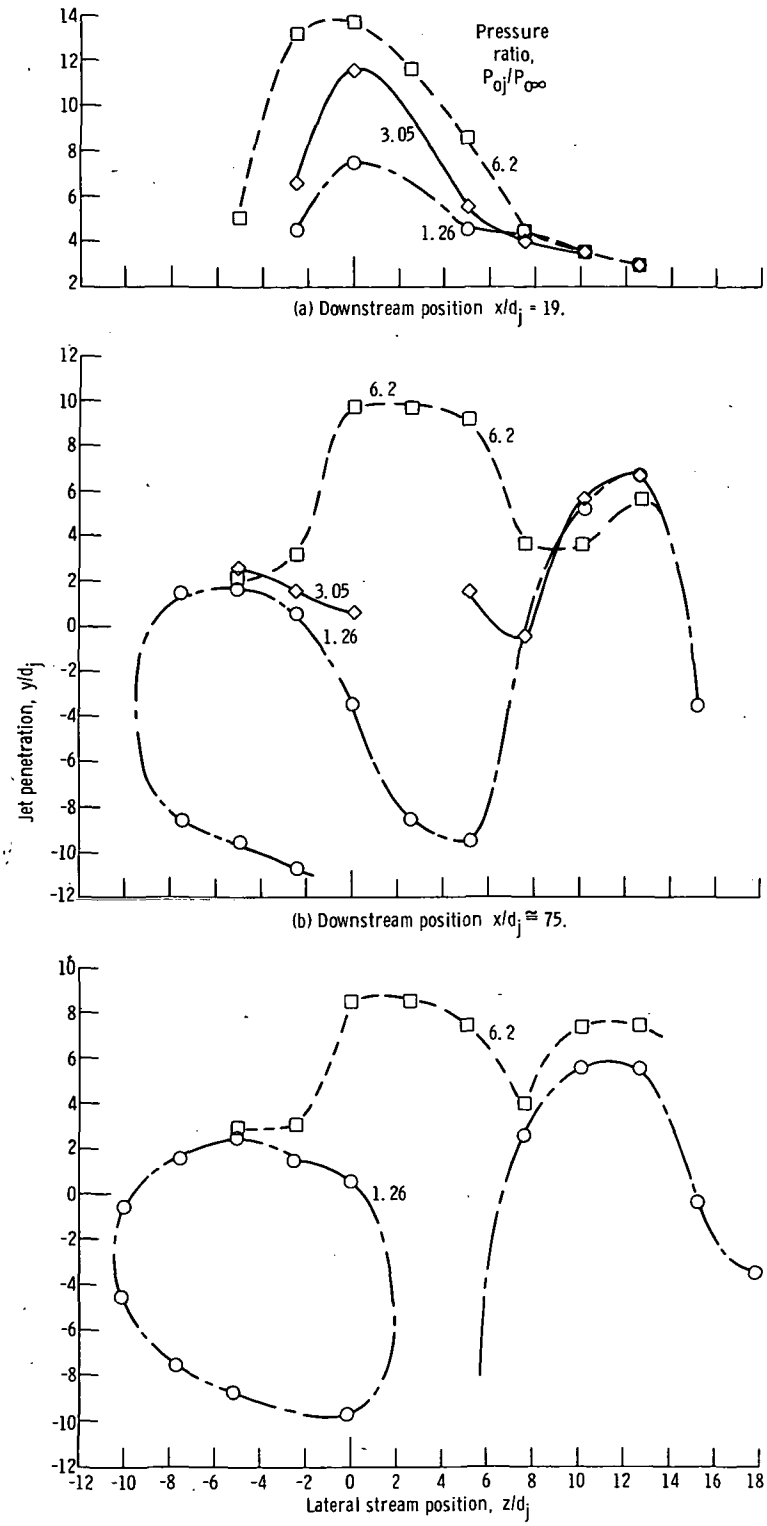

Figure 11. - Jet penetration as a function of pressure ratio. Mach number, 2.5; angle of attack, 14^0; model B.

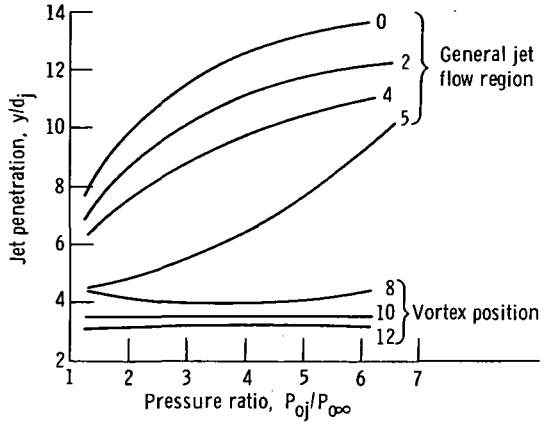

Figure 12. - Effect of injectant- to free-stream-pressure ratio on penetration at various lateral stream positions. Mach number, 2.5; angle of attack, 14^{0}; model B; downstream position $x/d_j = 19$.

Injector D

Two sets of data were obtained with this injector: one at 9.5^{o} angle of attack, the other at 17^{o} (fig. 13). (Injector D had a thickness ratio equal to that of B, as described earlier.) Comparison of these data with those of injector B (fig. 10(c)) shows that there is less penetration in the central jet region as well as in the vortex region. The lateral distribution also is compressed relative to injector B. The reduced lateral distribution is probably associated with the smaller base width of injector D. Since the total amount of helium is the same for both injectors, the local concentrations of helium adjacent to injector D must exceed those adjacent to injector B. In view of the fact that the drag of injector D is equal to that of B and that injector D's penetration and spreading are less than B's, injector B appears to be a more desirable geometry.

Various other schemes were tried in an effort to improve the penetration and spreading characteristics of the fuel injectors. None of these techniques yielded any improvement over injector B and will only be briefly described.

Subsonic leeward injection. - The injector shown in figure 3(a) was used. The penetration (see fig. 14) generally resembles that obtained with model B (fig. 10). The maximum penetration is 5.8 jet diameters in the central region compared to 7.5 for model B. In the vortex region, the value is 4.8 compared to 6.5 for injector B. Generally, the downstream behavior parallels that of model B. A stretching and breaking of the injectant plume appears to be occurring downstream.

Subsonic windward injection. - The injector is shown in figure 3(b). The penetration in the central jet region above the injector is seen to be low relative to injector B (see fig. 15(a)). In the vortex region, however, penetration is seen to be comparable to that of model B. An obvious helium deficiency is seen in the lower left quadrant region of the

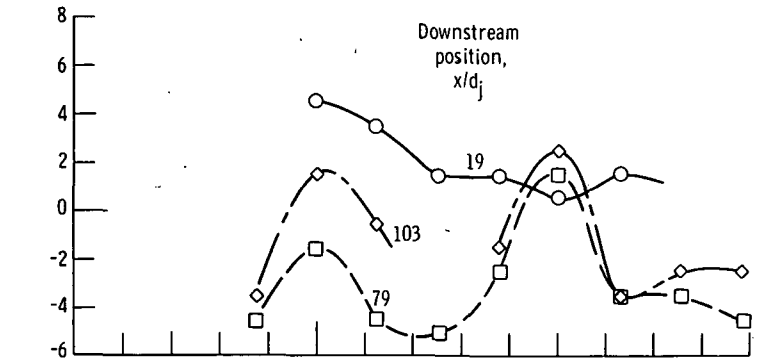

(a) Angle of attack, 9.5°.

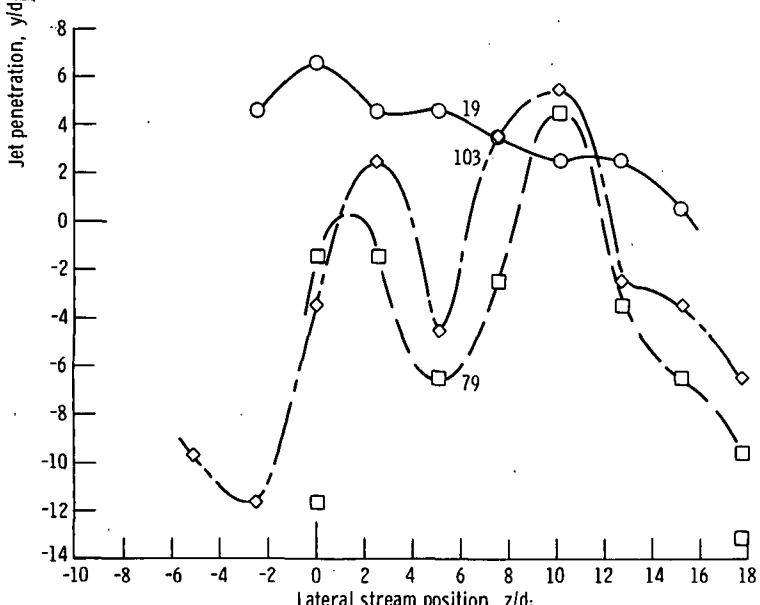

(b) Angle of attack, 17°.

Figure 13. - Jet penetration. Injector D; Mach number, 2.5; pressure ratio $P_{0j}/P_{0\infty} = 1.26$.

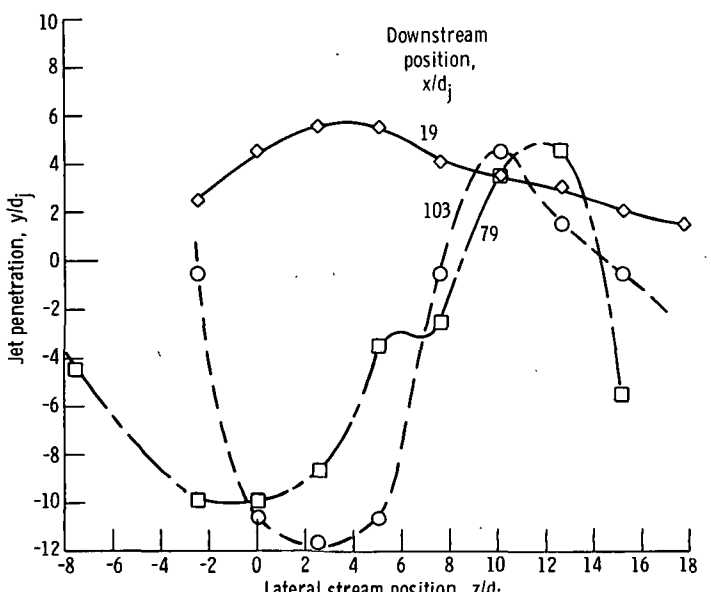

Figure 14. - Lateral distribution of injectant at various downstream positions. Mach number, 2.5; angle of attack, 14°; pressure ratio $P_{0j}/P_{0\infty} = 1.26$; six subsonic leeward orifices; model B modified.

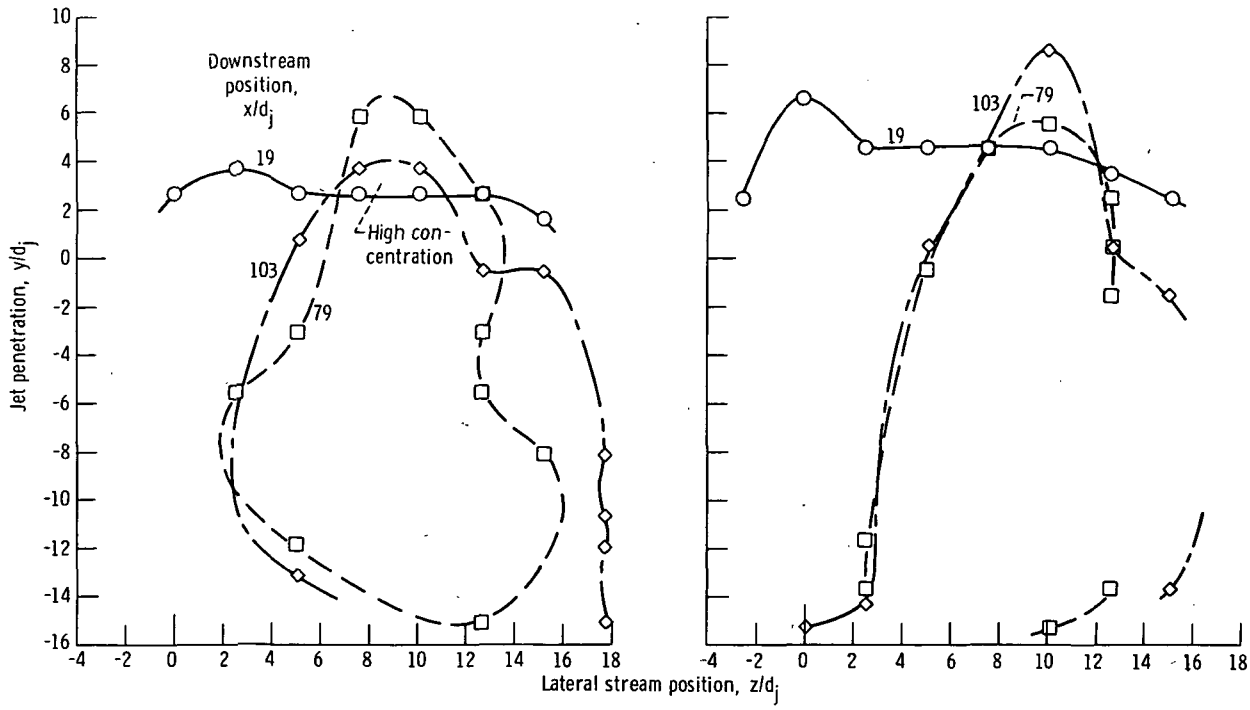

Figure 15. - Lateral distribution of helium at various downstream positions. Mach number, 2.5; pressure ratio $P_{0j}/P_{0\infty}$ = 1.26; three subsonic windward orifices; model B modified.

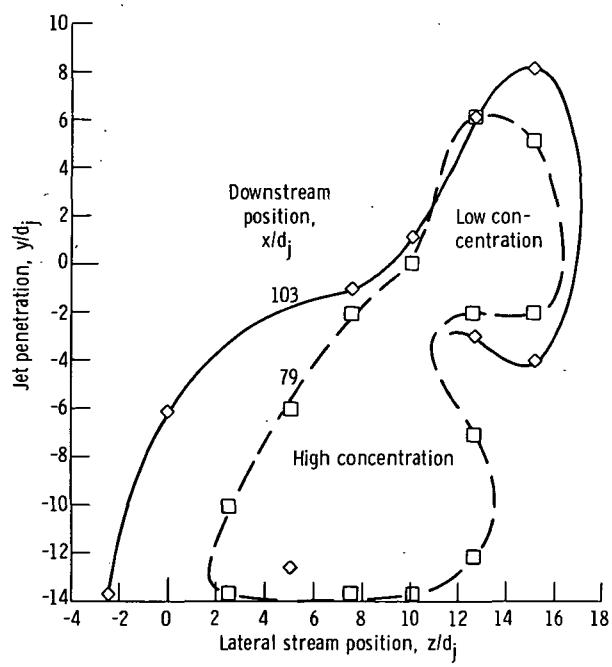

Figure 16. - Jet penetration at various downstream positions. Mach number, 2.5; angle of attack, 17°; pressure ratio $P_{0j}/P_{0\infty}$ = 1.26; model C.

flow field, that is, the lower part of the central jet region. Increasing the angle of attack to 18° (fig. 15(b)) produces greater penetration but it still does not allow any helium to fill the lower left quadrant region.

Subsonic windward injection through a sintered strip. - Results are shown in figure 16. The injector used was that shown in figure 2. At an x/d of 19 no helium was detected on the leeward side of the injector. This is in contrast with the results obtained prior to this study with greater injectant mass flow (ref. 6). As with the previous results, helium was found to be limited to the region to the right of the injection orifice. With this injector, the region above the trailing edge contained only a low concentration of helium. The majority of the helium flowed straight back from the sintered strip.

CONCLUDING REMARKS

The drag of several single-element delta-shaped fuel injectors was measured in a Mach 2 to 3.5 airstream. The injectors were oriented at 12° and 20° angle of attack. The dynamic pressure of the airstream was varied from 35.8 to 60.4 kN/m^2 (748 to 1262 psfa). In these tests, the injector drag was found to be strongly dependent on injector thickness ratio. The larger aerowing injector (model B) yielded drag values which were no larger than the smaller (i.e., surface area) aerowing configurations (C and D). In addition model B exhibited superior penetration and spreading characteristics.

Jet penetration was measured over the range for 20 to 123 orifice diameters downstream. The free-stream Mach number was 2.5 and the total-injection- to free-stream-pressure ratio was varied from 1.26 to 6.2. The injection pressure ratio was found to profoundly influence the penetration. Far field measurements of the penetration differed appreciably from measurements in the near field. Injector B, which yielded favorable drag characteristics, was also found to have the most desirable injectant distribution.

Lewis Research Center,
National Aeronautics and Space Administration,
Cleveland, Ohio, October 16, 1973,
501-24.

APPENDIX A

SYMBOLS

A	area
C_D	drag coefficient
D	drag force
d	orifice diameter
L	swept-edge length
l	chord length
M	Mach number
P_o	total pressure
p	static pressure
t	injector thickness
x	downstream distance
y	distance above injector surface (perpendicular to undisturbed free stream)
z	lateral distance
α	angle of attack
δ	thickness ratio, t/l
Λ	wing sweepback angle

Subscripts:

b	base
e	direction normal to leading edge
i	induced
in	inboard
j	injection
psa	projected side area
te	trailing edge
th	thickness
∞	free stream

APPENDIX B

DRAG CALCULATION

Linearized supersonic flow theory was used to calculate the drag of the four injectors (A, B, C, and D) shown in figure 1. For purposes of calculation the injectors were assumed to be infinite wings having a constant chord length as shown in figure 17(a).

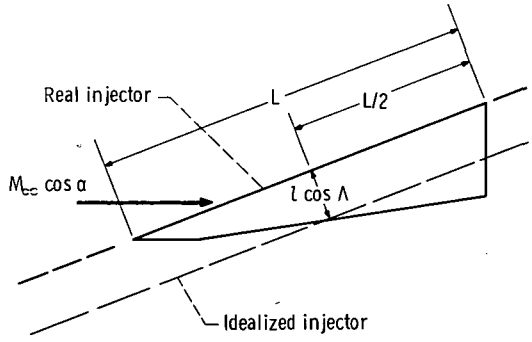

(a) Injector approximation.

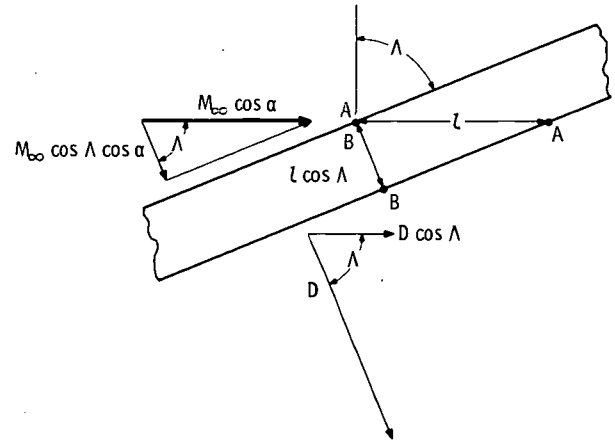

(b) Infinite wing, plan view.

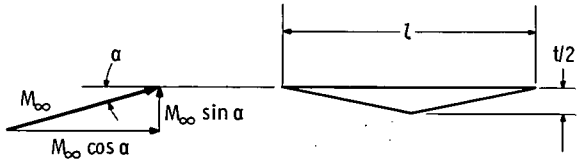

(c) Plane in direction A-A.

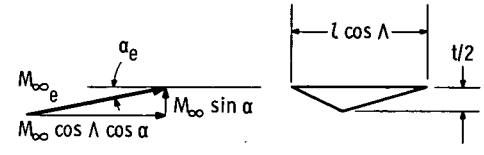

(d) Plane in direction B-B.

Figure 17. - Infinite sweptback wing and injector approximation for drag calculation.

The chord normal to the leading edge ($l \cos \Lambda$) was assumed equal to the chord at the midpoint of the swept edge of the delta wing. The method of small perturbations was employed to determine the various drag forces acting on the infinite wings.

Plan and cross-sectional views of the infinite sweptback wing are shown in figures 17(b), (c), and (d). The induced drag (or drag due to lift) coefficient is given by the expression

$$C_{D,i} = C_{D,i,e} \cos \Lambda (1 - \sin^2 \Lambda \cos^2 \Lambda)$$

where

$$C_{D,i,e} = \frac{4\alpha_e^2}{\sqrt{M_{\infty,e}^2 - 1}}$$

$$\alpha_e = \arctan\left(\frac{\tan \alpha}{\cos \Lambda}\right)$$

and

$$M_{\infty,e} = M_\infty \sqrt{1 - \sin^2 \Lambda \cos^2 \alpha} .$$

For the injectors at 12° angle of attack at Mach 2.0, the value calculated for $C_{D,i}$ was 0.204.

The thickness drag coefficient was determined from

$$C_{D,th} = C_{D,th,e} \cos \Lambda \left(\frac{M_{\infty,e}}{M_\infty}\right)^2$$

where

$$C_{D,th,e} = \frac{2\delta_e^2}{\sqrt{M_{\infty,e}^2 - 1}}$$

and

$$\delta_e = \frac{t}{l \cos \Lambda} = \frac{\delta}{\cos \Lambda}$$

For injectors A, B, C, and D the values of $C_{D,th}$ were 0.061, 0.078, 0.103, and 0.146, respectively.

The skin friction drag coefficient was assured to have a constant value of 0.006. The base drag was determined for the four injector models assuming that a Prandtl-Meyer expansion occurred over the trailing edge (90° expansion) and around the inboard edge (model A, 0° expansion; B, 5.7°; C, 10.3°; D, 16.5°). Base drag was then determined from the following expression:

$$D_b = (P_\infty - P_{te})A_b + (P_\infty - P_{in})A_{psa}$$

where the second term goes to zero for model A.

The total drag was determined from the summation of the drag coefficients multiplied by the planform area (twice the planform area for friction drag) of the four injectors. This in turn was nondimensionalized by the calculated drag of model A to give a drag ratio D/D_o as follows:

Model	Drag ratio, D/D_o
A	1.00
B	.93
C	.88
D	.83

The values of the drag ratio from the table are those which are plotted in figure 7.

REFERENCES

1. Metzler, A. J.; and Mertz, T. W.: Preliminary Results of Large Supersonic Burning Combustor Testing. J. Aircraft, vol. 9, no. 1, Jan. 1972, pp. 23-30.

2. Henry, J. R.; and Anderson, G. Y.: Design Considerations for the Airframe-Integrated Scramjet. Presented at the 1st International Symposium on Air Breathing Engines, Marseille, France, June 1972.

3. Povinelli, Louis A.; Povinelli, Frederick P.; and Hersch, Martin: Vortex Enhancement of Jet Penetration in Supersonic Flow. Paper 69-664, AIAA, June 1969.

4. Povinelli, Louis A.; Povinelli, Frederick P.; and Hersch, Martin: A Study of Helium Penetration and Spreading in a Mach 2 Airstream Using a Delta Wing Injector. NASA TN D-5322, 1969.

5. Povinelli, Frederick P.; Povinelli, Louis A.; and Hersch, Martin: Effect of Angle of Attack and Injection Pressure on Jet Penetration and Spreading from a Delta Wing in Supersonic Flow. NASA TM X-1889, 1969.

6. Hersch, Martin; and Povinelli, Louis A.: Jet Penetration into a Mach 2 Airstream Using Sweptback Injectors at Angle of Attack. NASA TN X-2319, 1971.

NASA-Langley, 1974 E-7662

NATIONAL AERONAUTICS AND SPACE ADMINISTRATION
WASHINGTON, D.C. 20546

OFFICIAL BUSINESS
PENALTY FOR PRIVATE USE $300

SPECIAL FOURTH-CLASS RATE BOOK

POSTAGE AND FEES PAID
NATIONAL AERONAUTICS AND SPACE ADMINISTRATION
451

U.S.MAIL

POSTMASTER: If Undeliverable (Section 158 Postal Manual) Do Not Return

"The aeronautical and space activities of the United States shall be conducted so as to contribute . . . to the expansion of human knowledge of phenomena in the atmosphere and space. The Administration shall provide for the widest practicable and appropriate dissemination of information concerning its activities and the results thereof."

—NATIONAL AERONAUTICS AND SPACE ACT OF 1958

NASA SCIENTIFIC AND TECHNICAL PUBLICATIONS

TECHNICAL REPORTS: Scientific and technical information considered important, complete, and a lasting contribution to existing knowledge.

TECHNICAL NOTES: Information less broad in scope but nevertheless of importance as a contribution to existing knowledge.

TECHNICAL MEMORANDUMS: Information receiving limited distribution because of preliminary data, security classification, or other reasons. Also includes conference proceedings with either limited or unlimited distribution.

CONTRACTOR REPORTS: Scientific and technical information generated under a NASA contract or grant and considered an important contribution to existing knowledge.

TECHNICAL TRANSLATIONS: Information published in a foreign language considered to merit NASA distribution in English.

SPECIAL PUBLICATIONS: Information derived from or of value to NASA activities. Publications include final reports of major projects, monographs, data compilations, handbooks, sourcebooks, and special bibliographies.

TECHNOLOGY UTILIZATION PUBLICATIONS: Information on technology used by NASA that may be of particular interest in commercial and other non-aerospace applications. Publications include Tech Briefs, Technology Utilization Reports and Technology Surveys.

Details on the availability of these publications may be obtained from:

SCIENTIFIC AND TECHNICAL INFORMATION OFFICE

NATIONAL AERONAUTICS AND SPACE ADMINISTRATION

Washington, D.C. 20546